Energy & Buildings 350 (2026) 116661

Contents lists available at ScienceDirect

Energy & Buildings

journal homepage: www.elsevier.com/locate/enb

Experimental assessment of wall thermal properties using an integrated response factor approach

Maja Danovska *, Davide Cassol, Ivan Giongo, Alessandro Prada

Department of Civil, Environmental and Mechanical Engineering, University of Trento, via Mesiano 77, Trento 38123, Italy

ARTICLE INFO

Keywords:
Thermal transmittance
Response factors theory
Periodic thermal properties
Numerical modelling
Experimental characterization
Hot-box test

ABSTRACT

Accurate determination of thermal parameters in building envelope components is crucial for evaluating energy performance. While response factor theory has been applied to accelerate the experimental characterization of steady-state thermal properties such as the U-value, periodic thermal properties remain underexplored despite their growing relevance due to global warming. This study presents a novel model based on response factor theory to characterize the unitary heat flux on the opposite side of a pulse solicitation as a function of time and four key parameters. A unified testing methodology is proposed, enabling simultaneous characterization of stationary and periodic thermal properties through a single hot box experiment. Key aspects of the setup, testing protocol, and data processing are detailed. The method was first validated via numerical simulations. Simulations, performed using a Finite Element Method, demonstrate the high accuracy of the proposed method in estimating both stationary and periodic thermal parameters with deviations under 5%. The method also showed resilience to boundary condition noise (mainly below ±10%). Following on from this point, experimental validation on an insulated wall confirmed the approach's effectiveness, with deviations under 10% compared to traditional decoupled methods. This approach offers a streamlined pathway for standardized thermal characterization assessment.

1. Introduction

The opaque building envelope plays a crucial role in overall energy performance, especially in minimizing heat loss during winter and mitigating overheating during summer. In cold season, high thermal insulation reduces heating demand and improves energy efficiency. Conversely, in summer, the envelope must act as a thermal buffer, limiting external heat gains, absorbing heat gains during peak hours and releasing it at night. This behavior mitigates indoor overheating and lowers cooling demand, which increasingly contributes to total building energy consumption [1].

While thermal resistance is the key parameter for winter performance, summer conditions require consideration of the envelope's thermal capacitance, that determines the envelope's ability to absorb and store heat gains, regulating indoor temperatures and preventing overheating. Achieving optimal performance year-round, whether designing new buildings or retrofitting existing ones, enhances building resilience against seasonal thermal variations, helping buildings adapt to climate challenges and supports energy sustainability. Strategies to enhance resilience include applying specialized materials such as Phase Change Materials [2–7] and the optimization of envelope stratigraphy [8–11]. The envelope can be leveraged actively [12–19], or passively [2–11], to improve operational flexibility, enabling energy flexibility and adjusting power demand dynamically [6,19]. This approach reduces energy consumption and CO_2 emissions. However, balancing energy flexibility with resilience is crucial to avoid trade-offs [6].

Recognizing that the envelope is more than a boundary between indoor and outdoor environments, it becomes essential to accurately quantifying its thermal properties. While analytical methods, as outlined in standards such as EN ISO 6946 [20] and EN ISO 13786 [21], are commonly used, they often assume uniform and constant material properties. These assumptions may not hold for real-world conditions [22,23]. Materials like timber have variable properties depending on grain direction, and hygroscopic materials exhibit moisture-dependent behavior, complicating standard calculations [24]. To address these limitations, numerical simulations are often employed. However, if material properties and input parameters are assumed rather than measured, results may not accurately reflect actual conditions. As demonstrated in [25], combining simulations with experimental data enables accurate thermal characterization, ensuring reliability even for complex wall assemblies.

* Corresponding author.
E-mail address: maja.danovska@unitn.it (M. Danovska).

https://doi.org/10.1016/j.enbuild.2025.116661
Received 18 July 2025; Received in revised form 14 October 2025; Accepted 28 October 2025
Available online 31 October 2025

Nomenclature

Variable	*Definition (unit of measurement)*
a	Peak flux fitting parameter (W m^{-2} K^{-1})
b	Shape factor fitting parameter (-)
c	Peak time fitting parameter (h)
c_p	Specific heat (J kg^{-1} K^{-1})
d	Starting time fitting parameter (h)
$\Delta\tau_{ie,fit}$	Time-shift (fitting output) (h)
$\Delta\tau_{ie}$	Time-shift, $\Delta\tau_{ie} = \Delta\tau_{ie,fit} + d$ (h)
ε^*	Cumulative percentage value (%)
f	Decrement factor (-)
φ	Unitary dynamic heat flux (W m^{-2} K^{-1})
φ_p	Unitary periodic heat flux (W m^{-2} K^{-1})
g	Heat flux offset fitting parameter (W m^{-2} K^{-1})
λ	Thermal conductivity (W m^{-1} K^{-1})
$\dot{q}$	Heat flux (W m^{-2})
ρ	Density (kg m^{-3})
τ	Time (h)
τ^*	Trial time (h)
t	Integration time (h)
$T_{a,i}$	Internal air's temperature (°C)
$T_{e,i}$	External air's temperature (°C)
T_p	Sinusoidal temperature (°C)
$\overline{T}_p$	Normalized sinusoidal temperature (-)
U	Thermal transmittance (W m^{-2} K^{-1})
y	Time (h)
Y_{ie}	Periodic thermal transmittance (W m^{-2} K^{-1})
Symbol	***Definition***
CLT	Cross Laminated Timber
DA	Decoupled Approach
e	Euler's number
erf	Error function
GA	Genetic Algorithm
INS	Insulated wall
ln	Natural logarithm
SNR	Signal-to-noise ratio

Experimental methods offer greater reliability and are typically conducted using a hot-box apparatus, which allows precise and accurate thermal assessment under controlled conditions. Stationary tests are widely standardized, especially for U-value measurements [26,27], though they can be time-intensive, up to 20 days for a single wall test [28]. The hot-box method has been widely used to measure U-values of different walls [29]. For summer performance assessment, no standardized procedures exist, though various studies have tested components under periodic conditions to evaluate uncertainties [30,31]. Research has explored periodic property determination through climate chamber testing. Studies like [32] optimized wall stratigraphy for improved indoor comfort, while others investigated how different forcing temperature shapes influence periodic responses [33–35]. Results suggest that step or triangular temperature variations can effectively replace sinusoidal waves in periodic tests, reducing experimental complexity. Maintaining stable internal conditions (temperature variations within 0.1 K) is crucial for accurate results. Some studies have extended periodic thermal property investigations using modified hot-box apparatuses to assess uncertainties [35], while others separately measured U-values and time shifts of insulated facades [36].

Traditionally, stationary and periodic thermal properties are determined through distinct and separate sequential tests. However, recent advancements aim to combine tests, reducing total testing time. A novel methodology based on Response Factors Theory [37] has been

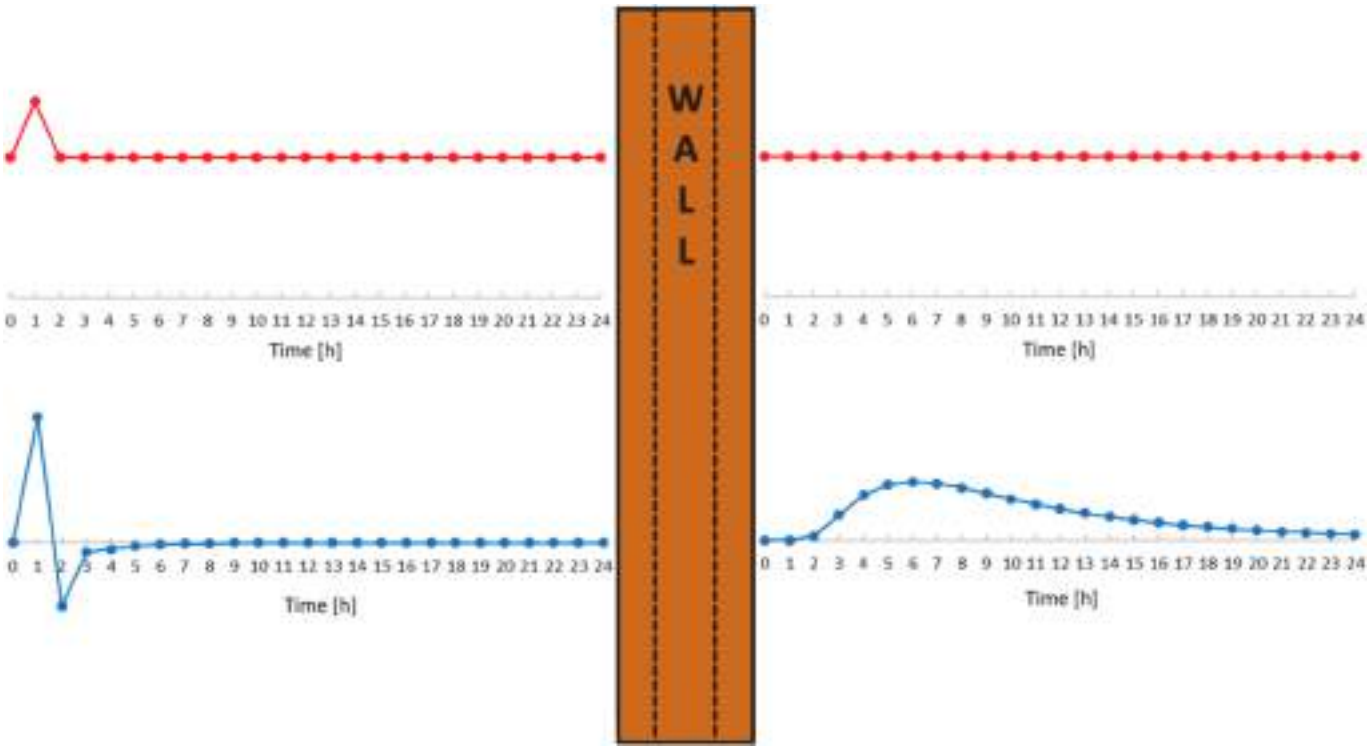

Fig. 1. Description of the response factors theory. The red curves represent temperatures over time, while the blue curves indicate the associated heat flux responses. (For interpretation of the references to colour in this figure legend, the reader is referred to the web version of this article.)

introduced, enabling U-value determination through a temperature pulse method. Fig. 1 illustrates the Response Factors test. This technique applies a triangular temperature pulse to one side of a wall while keeping constant conditions on the other. The resulting heat flux response, characterized by peaks on both the excited and non-excited sides, is described using a series of response factors: theoretical, infinite-time series representing the wall's thermal behavior. In practice, the series is truncated (e.g., to 24 terms) for feasibility. This approach bridges stationary and dynamic testing, enabling more efficient thermal characterization.

These series are widely used in dynamic simulation programs in the form of conduction transfer functions to solve transient heat conduction problems in opaque building envelope components. Additionally, directly utilizing response factors enables the determination of key wall characteristics, including its thermal properties. For instance, in [38] the response factors theory was applied in dynamic tests primarily to determine response factors rather than directly measuring the U-value using a hot-box apparatus. However, the study demonstrated that summing the first 50 terms of the response factors series resulted in thermal transmittance values deviating by 9.55% from the stationary value.

Similarly, [39] employed the dynamic approach to characterize walls using response factors, rather than focusing on U-value determination. The methodology was validated by comparing the summed response factors with the stationary thermal transmittance, achieving good agreement between the results. More recent studies [40,41] and [42] have extend this methodology to derive R-value of walls. Despite these advancements, no unified framework currently integrates dynamic and periodic evaluations. Some studies [43] experimented with changing the temperature forcing function from sinusoidal to impulsive solicitations to assess periodic thermal behavior. The impulse method provided a quicker transient analysis, though results were less accurate than the sinusoidal approach.

According to the state of the art, the impulse method is typically used to evaluate the thermal transmittance of walls under laboratory or in situ, conditions, or to determine dynamic responses through response factors. However, to the best of our knowledge, no studies have demonstrated its use for the comprehensive characterization of thermal performance of building components. This paper contributes to and advances the current literature by proposing a novel method that overcomes the traditional separation between steady-state and periodic tests, thereby reducing both testing time and energy consumption.

This study introduces a novel approach that relies solely on a single dynamic test, from which all thermal properties, including U-value, periodic thermal transmittance, time-shift, and decrement factor, can be extracted. This unified method offers substantial advantages in energy and time savings, particularly beneficial in manufacturing contexts, where wall stratigraphy can be adjusted in a timeframe comparable to production cycles.

To validate this approach, experimental data were collected using a hot-box apparatus on a polyurethane wall, complemented by numerical comparisons of three additional walls: a clay-brick masonry wall, a CLT wall, and an insulated wall. Furthermore, a sensitivity analysis was conducted to assess the impact of temperature boundary condition fluctuations, ensuring that this method remains applicable to hot-box setups where temperature stability is maintained within a controlled range.

2. Formulation of the unified dynamic test approach

The foundation of the proposed methodology lies in the response factors theory [37], which enables the evaluation of the unitary thermal response of an opaque building component. This is achieved by applying a unitary triangular pulse of temperature on the specific surface that wants to be analyzed [44], as shown in Fig. 1. This thermal response can be further elaborated to obtain significant information regarding the analyzed components.

In this work a mathematical model was firstly developed to express unitary heat flux on the opposite side of the solicitation (φ) as a function of the time (τ) and of four fitting parameters a, b, c and d as reported in Equation (1). The term "unitary heat flux" refers to the heat flux (in W m^{-2}) divided by a unitary temperature difference (i.e., 1 K), such that it represents the thermal response per unit temperature excitation. Fig. 2 illustrates the time evolution of the unitary heat flux and the fitting parameters are highlighted according to their influence on the function. Each parameter has a physical meaning: the parameter a (*peak flux*) is the maximum value of the heat flux, b (*shape factor)* affects the shape of the fitting function, c (*peak time*) is the time at which the maximum occurs starting point, and d (*starting time)* is the time at which the unitary heat flux marks the onset of non-zero heat flux. All the four parameters are defined as positive.

$$\varphi(\tau) = \begin{cases} 0 & for\ \tau \le d \\ a \cdot e^{-b \cdot \ln^2\left(\frac{\tau - d}{c}\right)} & for\ \tau > d \end{cases} \quad (1)$$

It is possible to compute the thermal transmittance of the analyzed component by integrating the unitary heat flux, as defined in Equation (1), over the interval from zero to infinity (see Equation (2))[44].

$$U = \int_0^{+\infty} \varphi(\tau)\, d\tau = \frac{a \cdot c \cdot \sqrt{\pi}}{\sqrt{b}} \cdot e^{\frac{1}{4b}} \quad (2)$$

The unitary periodic heat flux (φ_p) can be written as the product between the module of the periodical thermal transmittance (Y_{ie}) and a sine function of time, considering a phase shift ($\Delta\tau_{ie,fit}$) representing the delay with respect to the temperature solicitation (Equation (3)).

$$\varphi_p(\tau) = Y_{ie} \cdot \sin\left((\tau + \Delta\tau_{ie,fit}) \cdot \frac{\pi}{12}\right) \quad (3)$$

Y_{ie} and $\Delta\tau_{ie,fit}$ can be determined using the dynamic heat flux definition combined with the response factors theory [44,45,46,47], exploiting the superposition principle. A sinusoidal temperature solicitation T_p, with a 24-h period, can be expressed as a sum of unitary temperature pulses scaled according to the magnitude of the sinusoidal temperature function (Fig. 3). Hence, the periodic heat flux on the opposite side at time τ, can be expressed as a sum over t from 0 to infinity of a series of unit heat flux responses, each weighted by the normalized historical temperature values, as illustrated in Fig. 3. Therefore, φ_p can be expressed as:

$$\varphi_p(\tau) = \int_0^{+\infty} \varphi(t) \cdot \overline{T}_p(\tau - t)\, dt = \int_0^{+\infty} \varphi(t) \cdot \sin\left((\tau - t) \cdot \frac{\pi}{12}\right) dt \quad (4)$$

A relation correlating Y_{ie} and $\Delta\tau_{ie,fit}$ with the parameters a, b, c and d is derived by combining Equation (3) and Equation (4) obtaining the following correlation (see Equation (5)):

$$Y_{ie} \cdot \sin\left((\tau + \Delta\tau_{ie,fit}) \cdot \frac{\pi}{12}\right) = \int_0^{+\infty} \varphi(t) \cdot \sin\left((\tau - t) \cdot \frac{\pi}{12}\right) dt \quad (5)$$

Finally, by substituting (1) into (5) and dividing by the U-value, as defined in (2), Equation (5) can be rewritten as:

$$\frac{Y_{ie}}{U} \cdot \sin\left((\tau + \Delta\tau_{ie,fit}) \cdot \frac{\pi}{12}\right) = \frac{\int_d^{+\infty} a \cdot e^{-b \cdot ln^2\left(\frac{t-d}{c}\right)} \cdot \sin\left((\tau - t) \cdot \frac{\pi}{12}\right) dt}{\frac{a \cdot c \cdot \sqrt{\pi}}{\sqrt{b}} \cdot e^{\frac{1}{4b}}} \quad (6)$$

Finally, recalling that the ratio between Y_{ie} and U yields the decrement factor f, and simplifying the terms within the integral, the final formulation is obtained:

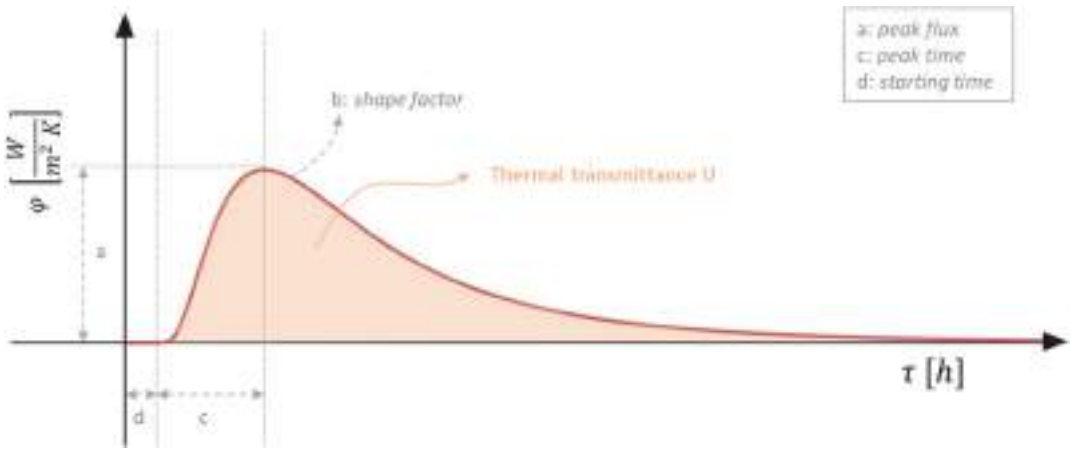

Fig. 2. Unitary heat flux φ obtained on the opposite side of the temperature solicitation.

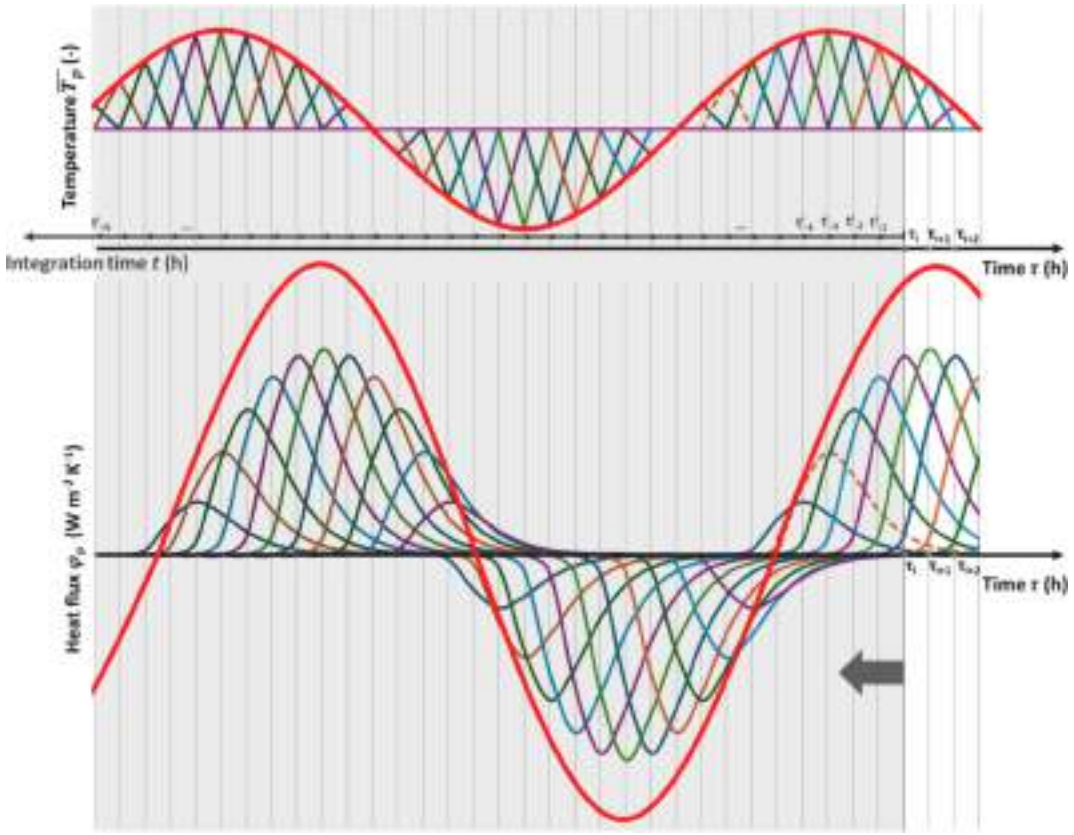

Fig. 3. Normalized periodic temperature forcing (red) as a sum of triangular pulses (top), and the wall's response (red) as the sum of individual pulse responses (bottom). (For interpretation of the references to colour in this figure legend, the reader is referred to the web version of this article.)

$$f \cdot sin\left(\left(\tau + \Delta\tau_{ie,fit}\right) \cdot \frac{\pi}{12}\right) = \int_{d}^{+\infty} \frac{\sqrt{b}}{c \cdot \sqrt{\pi}} \cdot e^{-b \cdot ln^2\left(\frac{t-d}{c}\right) - \frac{1}{4b}} \cdot sin\left(\left(\tau - t\right) \cdot \frac{\pi}{12}\right) dt \tag{7}$$

The decrement factor and the time-shift are determined numerically by integrating the right-hand side of Equation (7) for multiple values of t (ranging from 0 to 24 h), followed by a sinusoidal fit minimizing the error between the function on the left side of the equality and the calculated data. Fig. 4 show the generalized graphical output of the optimization procedure, illustrating the extent to which f and $\Delta\tau_{ie,fit}$ vary with the parameters b, c and d.

The decrement factor approaches 0 for low values of b or high values of c whereas it is not affected by parameter d. Conversely, parameter d is a constant time shift that is added to $\Delta\tau_{ie,fit}$. Physically, d represents the starting time of the heat flux response on the non-excited side, i.e. the delay before any non-zero signal appears after the temperature pulse. This delay is linked to the thermal diffusivity of the wall materials, which govern how fast heat propagates through the wall. As a result, the total time shift $\Delta\tau_{ie}$ can be considered as the sum of the intrinsic phase shift controlled by b and c and the constant offset introduced by d. The time-shift increases when c increases and has a strong dependence on c, especially for large values of b.

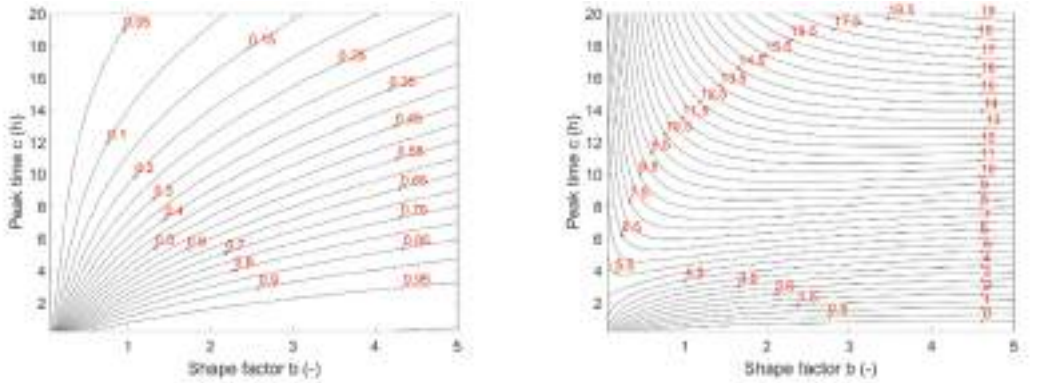

a) Decrement factor f (-) b) Time-shift $\Delta\tau_{ie,fit}$ - Starting time d (h) *

Note: * The time shift $\Delta\tau_{ie,fit}$ value is obtained by adding the starting time parameter d to the value read from the graph.

Fig. 4. Decrement factor f (−) expressed as a function of the parameters b (−) and c (h) and the Time-shift $\Delta\tau_{ie,fit}$ (h) expressed as a function of the parameters b (−), c (h) and d (h). Note: * The time shift $\Delta\tau_{ie,fit}$ value is obtained by adding the starting time parameter d to the value read from the graph.

3. The unified dynamic test procedure

The Unified Dynamic Test (UDT) procedure is structured into sequential phases: preliminary estimation of thermal parameters, definition of the testing setup and protocol, execution of the hot-box experiment, data processing with optimization, and validation. To describe the proposed methodology in detail, a flowchart has been added (Fig. 5). This helps in outlining key steps and highlights the streamline of the approach, which enables the simultaneous determination of both steady-state and periodic thermal parameters through a single test.

3.1. Preliminary estimation of the thermal parameters

A preliminary estimation of the thermal parameters of the opaque component is not required for the accuracy of the results, but it is important to optimize the testing protocol, mainly by defining a suitable test duration. Approximate values of U, f and $\Delta\tau_{ie}$ can be readily obtained from the literature or assumed as first-guess values. Based on these and an assumed value of d, parameters b and c can be estimated using the graphs in Fig. 6, while parameter a can be derived from Equation (1). When prior experience or specific literature data are available, the parameters *a, b, c* and *d* can also be directly estimated. If no reliable preliminary estimates are available, the test can simply be extended until equilibrium is reached, and the thermal parameters can still be correctly determined.

3.2. Definition of the testing setup and protocol

In general, the response factors theory is based on the unitary temperature pulse, however, in almost all conditions a unitary temperature increase cannot be detected by any real components, especially considering the sources of uncertainty and the low signal-to-noise ratio that would be encountered when measuring the heat flux resulting from

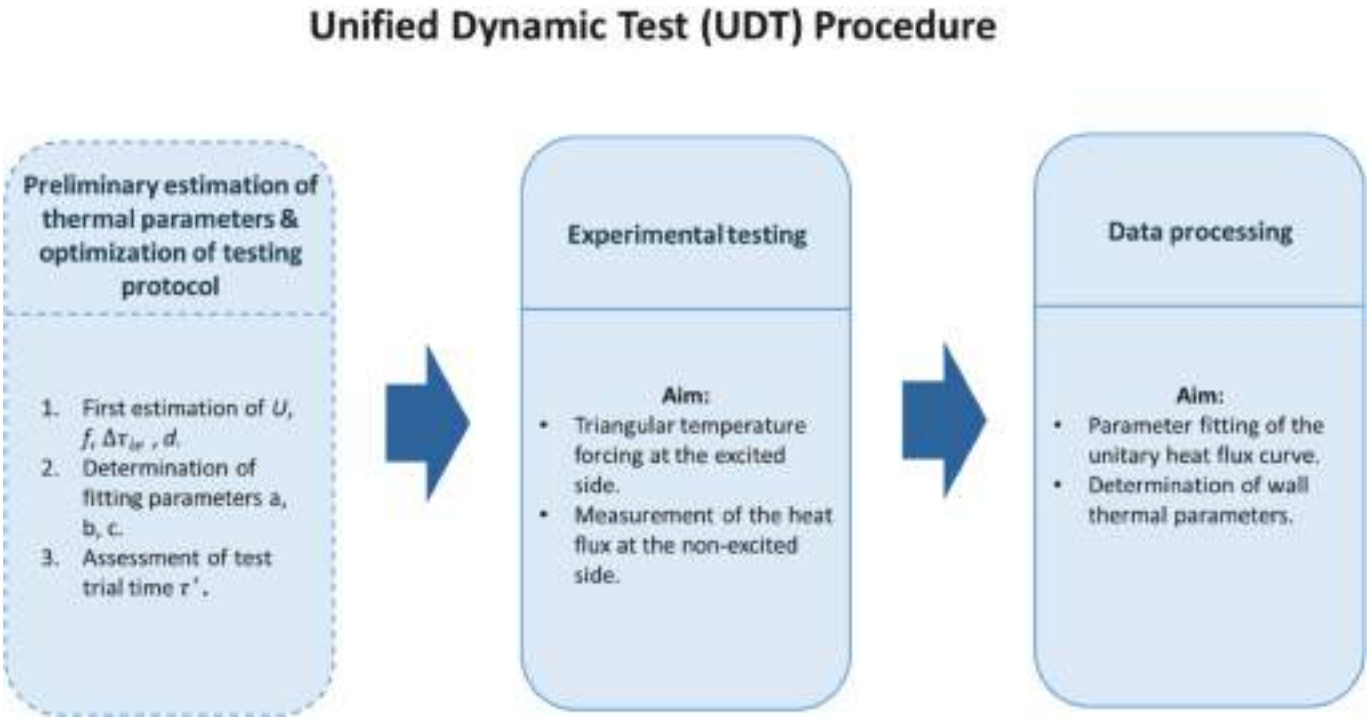

Fig. 5. Flowchart of the proposed Unified Dynamic Test (UDT) procedure.

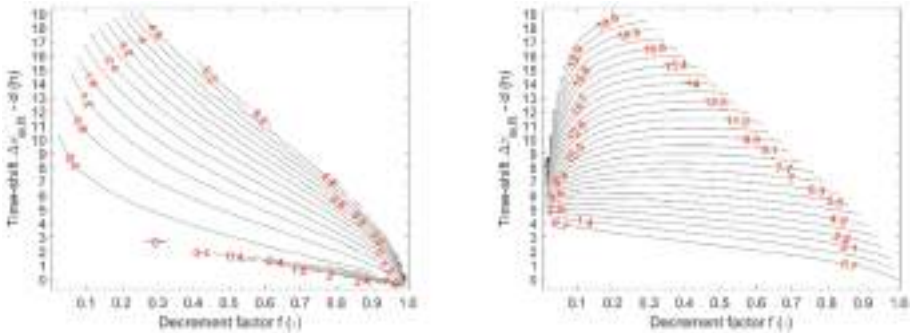

a) Shape factor *b* (-) b) peak time parameter *c* (h)

Fig. 6. Chart for first guess value estimation of parameters b (–) and c (h).

a unit temperature pulse. To address this limitation, the superposition principle allows for the application of a larger temperature pulse (ΔT). The resulting heat fluxes scale linearly with ΔT, enabling the generalization of the methodology also for real applications. A triangular temperature profile follows a general function in which the temperature starts from a certain value, it increases linearly by ΔT in one hour, and after that, it decreases within one hour by the same magnitude ΔT, returning to the initial temperature. Before the temperature pulse is applied, the component must be in thermal equilibrium, requiring a preliminary conditioning phase to ensure uniform temperature on both surfaces. While response factor theory implies an infinite duration to fully capture the system's response, in practice the test can be stopped once heat fluxes return to zero. By recalling Equation (1) that allows the computation of the U-value of a wall after a theoretical infinite test time, the U computed after a specific time called τ^* is the integral function of the unitary heat flux $\varphi(\tau)$ from 0 to τ^* as reported in Equation (8).

$$U(\tau^*) = \int_0^{\tau^*} \varphi(\tau)\, d\tau = \begin{cases} \tau^* \le d & 0 \\ \tau^* > d & U\cdot\left(\dfrac{1+erf\left(\sqrt{b}\cdot ln\left(\dfrac{\tau^*-d}{c}\right)-\dfrac{1}{2\cdot b}\right)}{2}\right) \end{cases} \tag{8}$$

where U is the asymptotic U-value for time approaching to infinity.

Equation (9) shows the dimensionless time required to reach a percentage value (ϵ_*) of the asymptotic thermal transmittance.

$$\frac{\tau^*-d}{c} = e^{\frac{1+\sqrt{b}\cdot k_*}{2\cdot b}},\ erf(k_*) = 2\cdot\epsilon_* - 1 \tag{9}$$

The non-dimensional time for different ϵ_* is plotted in Fig. 7, as a function of *b*. This plot can help the user to choose a suitable trial time, shorter than the theoretical infinite duration, that allows reaching the cumulative thermal transmittance value. It also can support post-

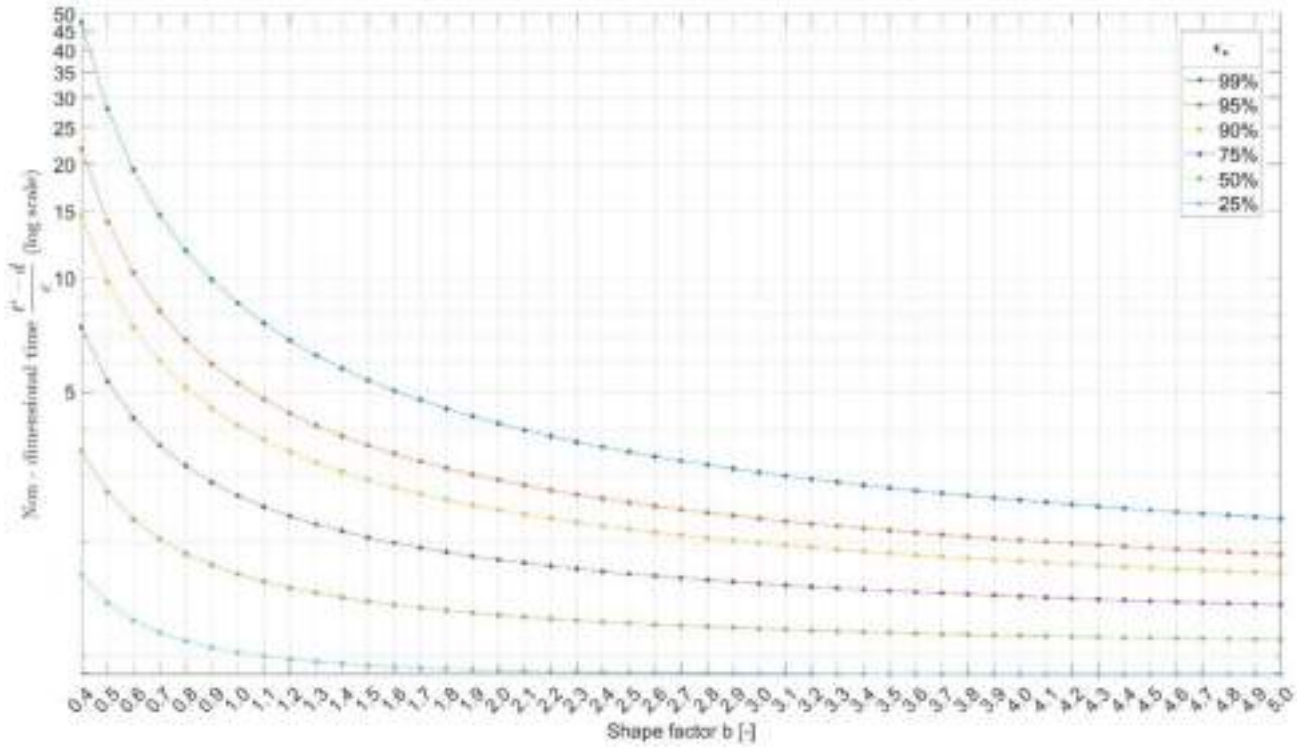

Fig. 7. Non-dimensional time as a function of the cumulative percentage ϵ_* and the shape factor b.

processing of the calculated U-value if the test ends early, to account for any missing data. Thus, it is possible to run the test for a period equal to the test time suggested by Fig. 7, which can be estimated by guessing at first a value of the parameter *b*, and by fixing a percentage of cumulative thermal transmittance at that specific time that can be considered as an acceptable value. This is a key aspect of UDT since it allows to save time, as well as energy, without running longer tests which do not add significant information to the heat flux series.

3.3. Experimental testing

The variable required for UDT is the heat flux on the surface opposite to the temperature pulse. Additional temperature and heat flux sensors can be installed to check the equilibrium conditions at the start of the test and the edge effects during the experiment. In fact, sensors should be installed on a portion of the component where boundary effects are minimized and in a representative area, usually this is in the central part of the component. Regarding the acquisition time, a 1-minute acquisition is regarded as a sufficient time to detect variations in temperature and heat flux which are consistent with the macroscopic thermal phenomena occurring across building components.

During the experimental run, it is possible to supervise some control variables in terms of both surface temperature and heat fluxes. Average temperatures on both sides of the analyzed component should be maintained equal considering the uncertainty of the measurements, as well as the stability of the equipment to apply proper boundary conditions to the component. Temperature probes allow to monitor the boundary conditions. With heat flux meters it is possible to control heat flux values, which should evolve around zero value. Possible offsets different than zero are possible, especially under experimental conditions and this does not compromise the proposed methodology. However, such offsets should not be significant with respect to the maximum value of the thermal responses, especially of the one on the opposite side of the excitation (that is, about 10 – 15% of the maximum value). Higher values may compromise the experimental results and further verifications must be carried out either on the heat flux sensors with a calibration procedure to correct such offsets or on the stability of the equipment to impose the boundary conditions, e.g., hot-box apparatuses.

3.4. Data processing

After measuring or retrieving heat fluxes on both surfaces, data must be processed. First, heat fluxes are divided by the magnitude of the temperature pulse to obtain a unitary heat flux series ready to be further elaborated by the optimization algorithm. The core part of the proposed methodology is the two-step optimization procedure aiming at determining, at first, fitting parameters of the unitary heat flux at the non-excited side, and after that, the time-shift and the periodic thermal transmittance. A Global Optimization approach was selected for the curve fitting of the unitary heat flux. Specifically, a Genetic Algorithm (GA) was chosen over the simple gradient-based optimization tool whose main disadvantage is the extremely high sensitivity to the choice of the initial point. Such method could converge prematurely during the optimization procedure, and they may not find a global optimum. The structure of the GA consisted in minimizing a fitness function, which in this case was chosen to be the root mean square error between the unitary heat flux and its fitting function. A key advantage of curve fitting lies in its ability to enhance signal clarity by effectively reducing measurement noise. This feature is particularly important in experiments where noise can significantly affect the accuracy of the results. This noise filtering process enhances the overall quality of the measurements, leading to more accurate characterization. Regarding the optimization parameters of the GA, the population size was set equal to 100 and a maximum of 2000 generations. Crossover probability was set to 0.8 and the mutation one was taken as a default value of the algorithm. The optimization terminated when the best solution converged within a tolerance of 10^{-6} and a limit of 500 stall generations. The next step concerns the numerical solution of Equation (5). This can be viewed as an optimization problem aimed at estimating the periodic thermal transmittance and the time-shift. For this purpose, the *fminsearch* algorithm [48] was selected since the nature of the optimization problem characterized by a sinusoidal function does not require searching for a specific local minimum, as in the previous step.

4. Validation

4.1. Numerical validation

A series of simulations were performed in COMSOL Multiphysics® [49] to initially validate the UDT procedure. Three different walls namely (1) a clay brick masonry wall 25 cm thick, (2) a cross laminated timber (CLT) wall with thickness of 10 cm and (3) a third wall composed of 12 cm polyurethane-based rigid foam insulation (INS) were simulated. The walls were selected to represent a range of different thermal behaviors, both in stationary and in transient regimes. Thermal properties of the analyzed walls are summarized in Table 1. Specifically, the thermal resistances of the three walls are 0.313 m^2 K W^{-1} for the clay brick masonry wall, 0.833 m^2 K W^{-1} for the CLT wall and 4.615 m^2 K W^{-1} for the insulation wall. The thermal capacitances are 1.51 MJ m^{-3} K^{-1} for the clay brick masonry wall, 0.67 MJ m^{-3} K^{-1} for the CLT wall and 0.05 MJ m^{-3} K^{-1} for the insulated wall.

Three different simulations were conducted for each wall. The first was a stationary simulation with fixed temperature boundary conditions equal to 20 °C, at the internal side, and 0 °C at the external side. Results of the simulation led to the determination of the U-value of each component. Such value was taken as a reference for the testing of the proposed methodology.

A second simulation was run in a periodic regime to evaluate the periodic thermal properties of each wall. A sinusoidal temperature solicitation with average value equal to 16 °C, a semi-amplitude of 10 K and a period of 24 h was applied on the external side. The internal air temperature was kept equal to 16 °C. The simulation was conducted for 10 days to stabilize the periodical signal. The aim was to compute Y_{ie}, $\Delta\tau_{ie}$ and f using standard equations commonly applied in the analysis of periodic thermal behavior.

Finally, simulations were run by applying a triangular temperature pulse on one side of the wall, called external or excited side. The temperature magnitude was chosen equal to 10 K, to have a considerable signal at the opposite side of the wall. Simulations continued for at least 4 days and it appeared to be a sufficient time after which the heat flux at the non-excited side reaches zero.

The three numerical models were solved with a Backward Differentiation Formula solver and a relative tolerance equal to 10^{-3} for the stationary solver, while for the periodic and the dynamic regimes, the Runge-Kutta solver was adopted with a relative and an absolute tolerance equal to 10^{-4} and 10^{-5}, respectively. By previously conducting a sensitivity analysis on the mesh, the normal size mesh was selected for all regimes of the clay brick masonry wall, while for the cross-lam and the insulated wall in the dynamic regime was necessary to adopt a finer mesh. As for the experimental outcomes, the Genetic Algorithm developed in MATLAB® [50] environment was exploited to find both fitting parameters and thermal properties.

Table 1
Thermo-physical properties of adopted materials in the numerical model.

Material	Density (kg m^{-3})	Thermal conductivity (W m^{-1} K^{-1})	Specific heat (J kg^{-1} K^{-1})
Clay brick masonry	840	0.800	1800
CLT	420	0.120	1600
INS	35	0.026	1464

4.2. Noisy boundary conditions

A further analysis was conducted focusing on the influence of the noise signal on the whole methodology, by applying a random signal (i.e., white noise) to the triangular temperature solicitation, as well as to the internal temperature, and by assessing again the four thermal parameters. The noise was defined as a zero mean random function with an amplitude within ±1 K. The noise was defined as a zero-mean random function with increasing magnitude of the semi-amplitude, from 0 to 1 K with a temperature step of 0.1 K. The temporal frequency of the noise was set to 1 min, corresponding to the acquisition time step of the temperature measurements. Such noise amplitude is consistent with noise in hot-box apparatuses which usually are of the order of magnitude of ±0.1 K, thus, significantly below the maximum value set in the sensitivity analysis. Nevertheless, in field applications, larger disturbances may occur, but these require shielding or dedicated instruments, which are beyond the scope of this study. The analysis was conducted in three stages to isolate and then combine the effects of noise on the boundary conditions: (i) noise applied only to the external air temperature, (ii) noise applied only to the internal air temperature, and (iii) noise applied simultaneously to both (Fig. 8).

The effect of the noise was evaluated at a first level on the curve fitting, and after that, on the estimation of the wall thermal parameters. In this analysis of the noise the same optimization approach of the free-noise analysis described earlier was adopted, both for the determination of the fitting parameters and for thermal properties.

The heat flux at the non-solicitated side under noisy boundary conditions was fitted, and fitting's parameters were determined per each noise level and thermal parameters were estimated. To enhance the statistical representativity of this analysis, 10 simulations were run with 10 different noise series for each noise magnitude and for each wall.

4.3. Experimental validation

An experimental validation process of the proposed methodology was performed as well using results obtained from an experimental campaign conducted on a polyurethane-based rigid foam insulation insulated wall with thickness equal to 12 cm. The material was chosen according to the numerical validation for consistency purposes. Experimental tests were conducted in the *Sustainable Energy Laboratory* at the University of Trento by means of a hot-box apparatus (Fig. 9). Three different tests were conducted, studying the behavior of the wall in the stationary, periodic and dynamic conditions. The outcomes of stationary and periodic tests were used as reference for the validation of the proposed methodology which was applied by means of the dynamic test.

In particular, the stationary test was performed with fixed temperature boundary conditions equal to 25 °C (hot chamber) and 5 °C (cold chamber). The periodic test was conducted in a periodic regime in which the external air's temperature was forced to follow a sinusoidal function with average temperature equal to 16 °C, semi-amplitude of 10 K and a period of 24 h. The opposite side was kept constant with a temperature equal to 16 °C. The dynamic test was conducted using a triangular profile with a magnitude of 10 K which was set to the external air's temperature. Such thermal profile develops in a total of 2 h after going back to 16 °C, as the temperature of the internal chamber. For each test, surface temperatures and heat fluxes were recorded with a time-step of 1 min by means of a Keysight DAQ970A data-acquisition system (voltage accuracy ±0.011 % at 100 mV range; resistance accuracy ±0.012 % at 100 Ω range) by installing thermocouples (Type-T, accuracy: ±1.07 °C), Platinum-Resistance thermometers (Pt-100, accuracy: ±0.24 °C) and heat flux meters (Model: HF-30S EKO Instruments, Sensitivity: 100 μV W^{-1} m^2) as reported in Fig. 10. Thermal transmittance and periodic thermal parameters were computed using both the UDT method and, separately, through two different test procedures consistent with commonly adopted approaches. The dynamic response of the wall in terms of experimental heat flux obtained at the opposite side of the solicitation was fitted by means of Equation (1). Since the experimental dynamic heat flux might not reach zero for longer time, an additional parameter is added in the fitting function. This parameter expressed the zero offset in the heat flux caused by a non-zero temperature difference between surface and air or by a not-proper calibration of the zero point of the heat-flux meters. A custom MATLAB® code was written to elaborate experimental results and to test the proposed methodology by running the optimization algorithm previously described. In this way, results from the single proposed methodology were compared with results of thermal parameters computed separately.

5. Results

5.1. Numerical validation

Fig. 11 compares the simulated heat flux against the fitted functions for the clay brick masonry wall. The left panels mark the simulation time τ* at which 99% of the theoretical U-value is reached, while the right panels zoom in on the heat flux around τ*, showing the corresponding truncated-series fitting with updated parameters. Graphical results show excellent agreement between the simulated heat flux and the fitting function. The same analysis was also repeated for the other two walls, yielding similar behavior. However, as the thermal capacitance of the wall decreases, the time τ* naturally decreases as well.

Table 2 presents the results of the numerical validation, comparing outcomes of the unified dynamic test (UDT) procedure with respect to the reference simulated tests, where parameters are computed separately. The table also includes results for the unified dynamic test procedure applied to a truncated heat flux series (UDT*). Deviations are generally small across all wall types, with the largest differences observed for the insulated wall, especially in U and Y_{ie}. Over the full time series, deviations are negligible for the clay brick and CLT walls, remaining within ±1%, which supports the method's reliability. For the insulated wall, slightly higher deviations are observed, with the largest being -3.4% for the corrected time shift. Other parameters stay within ±2%, well below the typical measurement uncertainty of ±10%. The UDT* approach yields result nearly identical to the full series, confirming the method's robustness and the adequacy of early truncation without significant loss of accuracy, although it may significantly reduce testing time.

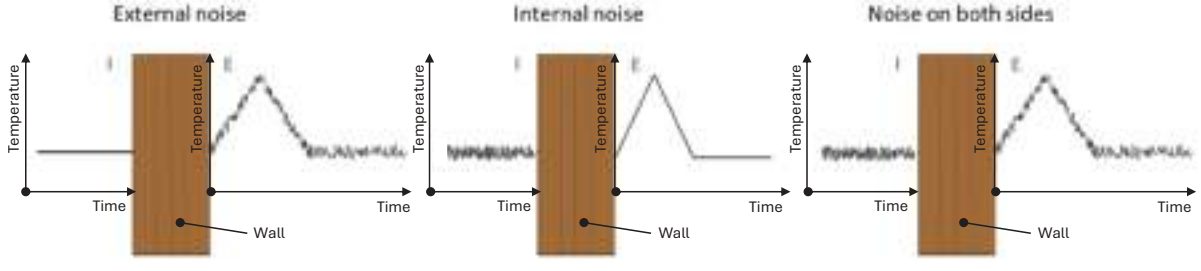

Fig. 8. Application of the noise on the temperature profiles for the external, internal and both case noise.

Fig. 9. Hot-box apparatus.

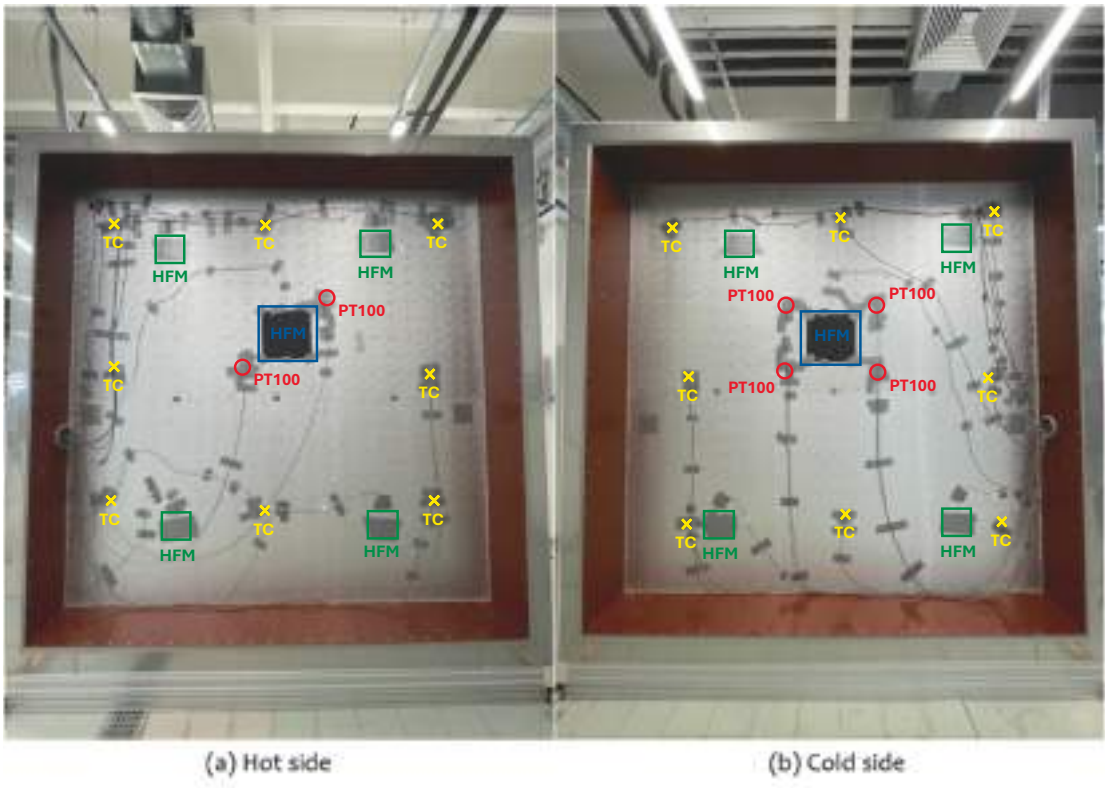

Fig. 10. Analyzed wall specimen with the data-acquisition system (sensors) installed on each surface of the insulated wall. Sensors description: heat flux meters (HFM); thermocouples (TC) and platinum thermal resistances (PT100) for the temperature measurement.

5.2. Noisy boundary conditions

Fig. 12 shows results of the maximum percentage deviations of the estimated thermal properties among the 10 simulation runs for each noise magnitude. Percentage values were computed considering parameters estimated without the noise. Results show that a noisy temperature in the boundary conditions impacts the estimation of key thermal properties significantly. The effect depends on both the noise magnitude (i.e., signal-to-noise ratio) and the side of application.

As noise increases, uncertainty grows, reflected by a greater percentage deviation. When noise is applied only on the external side (the triangle marks), its influence is minimal across all walls, with deviations within +5%. In contrast, a noisy temperature on the side where heat flux is measured (circle marks) leads to significantly higher errors. Finally, when both sides have noisy boundary conditions, as in real conditions, uncertainty generally increases further as reported with the cross marker in the plot.

An exception is seen for the CLT wall and the insulated wall, where internal noise alone produces a slightly higher error in U-value estimation than the both-sides case. This could be due to a partial compensation effect between the independently applied internal and external noise signals.

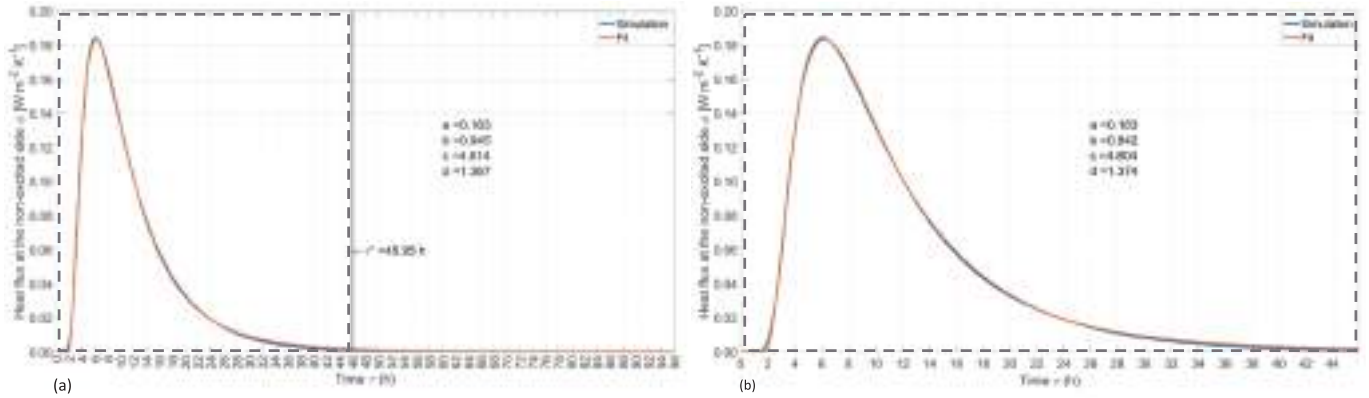

Fig. 11. (a) Heat flux at the non-excited side obtained from the dynamic simulation as a function of the time. (b) Detail on the range from 0 to τ^* corresponding to $\varepsilon^* = 99\%$.

Table 2
Estimated thermal parameters from the Unified Dynamic Test procedure considering the whole heat flux series (UDT) and the truncated one (UDT*).

Wall	Thermal parameters	Decoupled approach (reference)	UDT	UDT*	UDT Deviations (%)	UDT* Deviations (%)
Clay brick masonry	$U\ (W\,m^{-2}\,K^{-1})$	2.091	2.098	2.099	+0.32	+0.42
	$Y_{ie}\ (W\,m^{-2}\,K^{-1})$	0.894	0.900	0.900	+0.71	+0.64
	$f\ (-)$	0.428	0.429	0.429	+0.39	+0.22
	$\Delta\tau_{ie}\ (h)$	7.37	7.36	7.35	-0.06	-0.06
CLT	$U\ (W\,m^{-2}\,K^{-1})$	1.001	0.993	0.993	-0.79	-0.81
	$Y_{ie}\ (W\,m^{-2}\,K^{-1})$	0.853	0.845	0.845	-0.88	-0.88
	$f\ (-)$	0.852	0.851	0.851	-0.09	-0.07
	$\Delta\tau_{ie}\ (h)$	3.28	3.31	3.31	+0.91	+0.89
INS	$U\ (W\,m^{-2}\,K^{-1})$	0.209	0.206	0.206	-1.65	-1.65
	$Y_{ie}\ (W\,m^{-2}\,K^{-1})$	0.204	0.200	0.199	-1.83	-1.89
	$f\ (-)$	0.974	0.972	0.972	-0.19	-0.19
	$\Delta\tau_{ie}\ (h)$	1.43	1.39	1.39	-3.29	-3.29

For the clay brick masonry wall, the U-value estimation remains highly stable under external-side noise, with deviations below +5% due to the wall's natural filtering effect. When noise is applied to the internal side, uncertainty increases, with errors reaching + 11 %. The largest errors occur when both sides are noisy, reaching +16%. Assuming a typical U-value measurement uncertainty of ±10%, boundary temperature noise up to ±0.7 K can be tolerated before this threshold is exceeded in the "Internal" and "Both" cases.

Errors are generally smaller in the periodic thermal transmittance and time-shift estimation, especially at higher noise levels. The smallest errors are observed in time-shift estimation, which is closely linked to the timing between the external temperature peak and the internal heat flux response.

For the CLT wall, uncertainties are consistently smaller than those of the clay brick masonry wall. Although errors increase with noise semi-amplitude, they remain within +10% for all thermal parameters. This suggests that walls with CLT-like thermal properties are more resilient to boundary temperature noise than more massive constructions like clay brick masonry.

For the insulated wall, which has higher thermal resistance and lower mass, similar error trends appear with increasing noise magnitude. Errors grow with noise amplitude, especially for the "Internal" and "Both" cases, while the external noise impact remains negligible. The U-value deviates up to about +10.5% at the highest noise level. Periodic thermal transmittance and corrected time-shift follow similar patterns, with the time-shift showing a tendency to be overestimated up to +12% (the highest deviations obtained among the walls and the sides of the noise application).

5.3. Experimental validation

The results of the simulated tests identified the insulated wall case as the most critical, leading to greater uncertainty in the UDT outcomes. For this reason, the experimental validation was carried out on the insulated wall. Fig. 13 shows the unitary heat flux on the non-excited side of insulated wall as a function of time expressed in hours, along with the best fitting of experimental data. Fig. 13 (a) provides a detail view of the heat flux truncated in correspondence of time τ^* ($\epsilon_* = 99\%$) together with the new optimized parameters over the shorter period. The fitted curve closely reproduces accurately the real behavior of the insulated wall, despite some disturbances. An additional parameter (g) is introduced when dealing with experimental data, to account for the zero-offset error in heat flux measurements, as specified in the sensor manufacturer's datasheet. In this experiment, $g = -4{\cdot}10^{-3}\ W\,m^{-2}$, corresponds to approximately the 3% maximum heat flux measured. Such parameter does not enter inside the optimization problem for the determination of the thermal parameters. The blue curve in the left chart refers to the initial test time, i.e. 49 h. However, the time series can be truncated based on the trial duration computed in Fig. 6. Specifically, setting the parameter ϵ_* to 99% yields a corresponding trial time of 5.34 h. The remaining terms of the series can then be neglected. Fig. 13 (a) shows results of the first-optimization step with the truncated time series at τ^*. Notably, the parameter estimates remain largely unaffected by the truncation.

Table 3 presents experimental validation comparing thermal parameters from the single approach with the decoupled method. The full series UDT shows good agreement with deviations below ±7% for all parameters. Measurement uncertainty for the decoupled method was

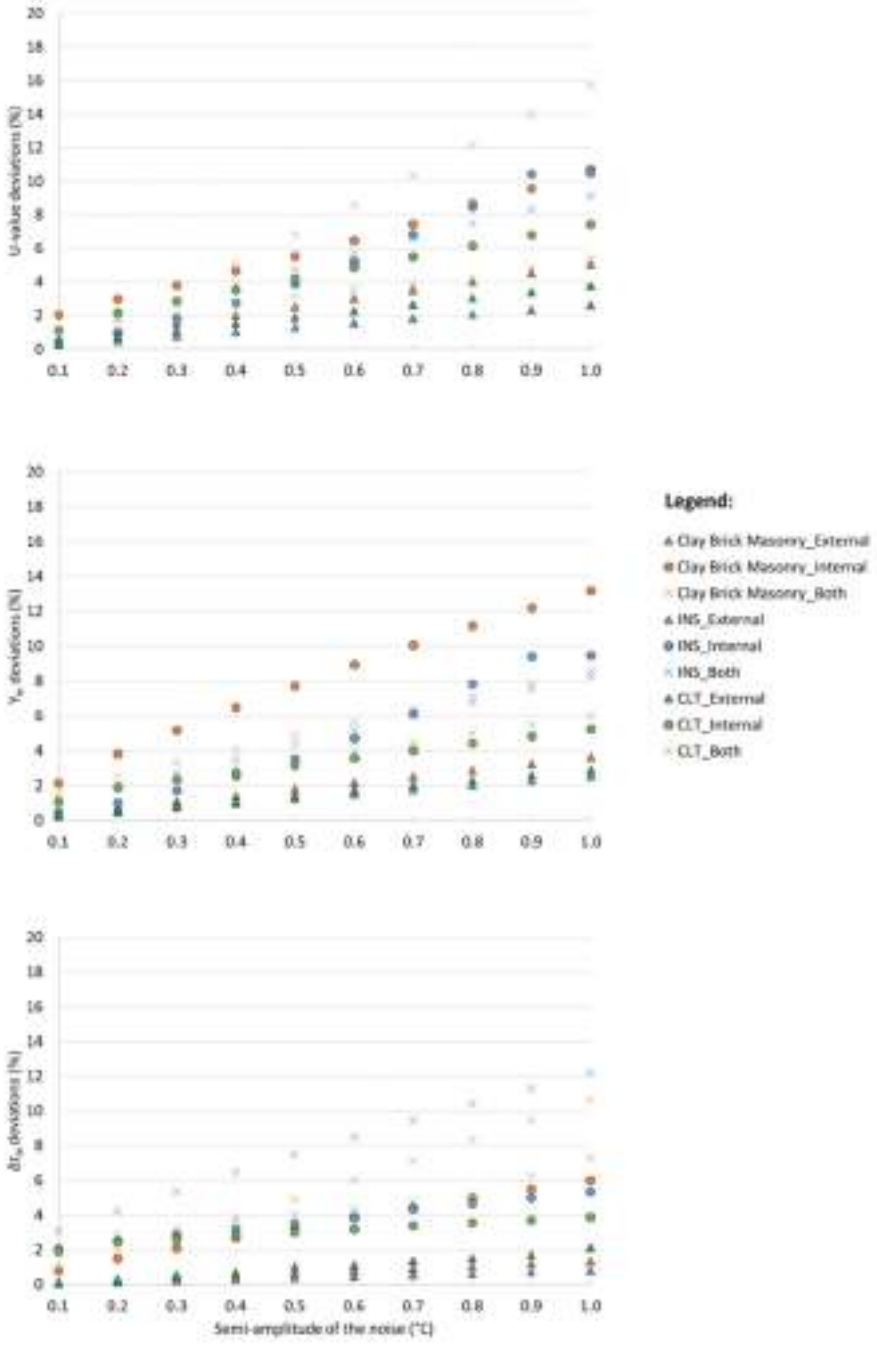

Fig. 12. Impact of the temperature noise on the UDT outcomes.

estimated via error propagation. The largest deviation occurs in the corrected time-shift, mainly due to underestimation of the parameter d in the optimization. Other parameters deviate less than ±4%. Using the truncated series does not affect results, demonstrating that trial test time estimation can significantly reduce test duration and energy use without significant accuracy reduction.

6. Conclusions

This study presented a Unified Dynamic Test (UDT) procedure that enables the simultaneous determination of thermal transmittance and time-shift parameters of building envelopes using a single experimental test. Unlike conventional approaches, which require multiple protocols and extended durations, the proposed methodology integrates analytical modeling, dynamic simulations, and optimization techniques into one compact framework.

The main outcomes can be summarized as follows:

- The method provides both U-value and dynamic parameters (time shift and periodic thermal transmittance) in a single experiment, greatly reducing testing time.
- The fitting procedure acts as a noise filter, ensuring robustness against measurement disturbances; deviations remained below 5% under typical noise levels and below ±10% even in worst-case scenarios.
- The methodology was tested under varying levels of noise to assess its robustness. Outcomes remain accurate despite external disturbances, with deviations remaining below 5%.

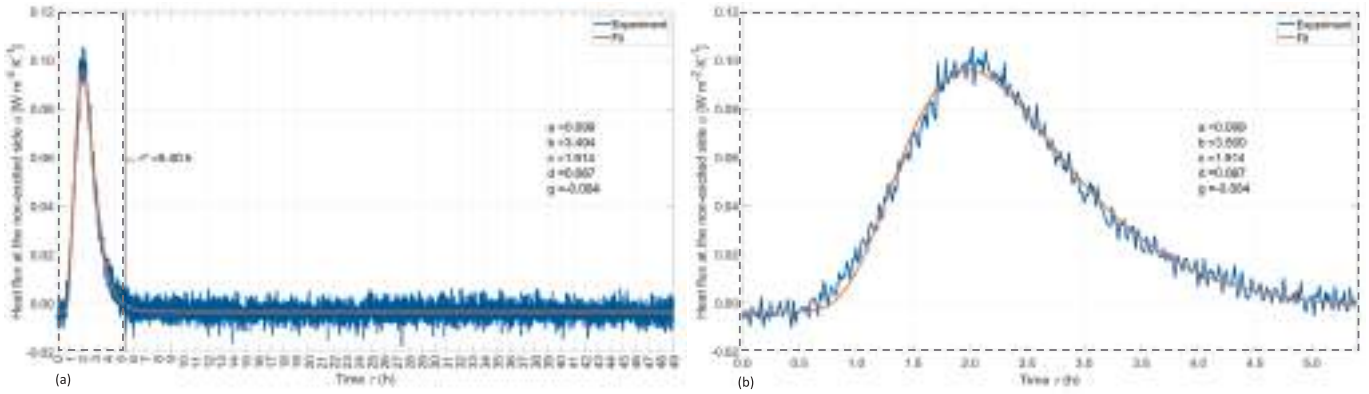

Fig. 13. (a) Heat flux at the non-excited side obtained from the dynamic simulation as a function of the time. (b) Detail on the range from 0 to τ* corresponding to ε* = 99%.

Table 3
Experimental thermal parameters from the Unified Dynamic Test procedure considering the whole heat flux series (UDT) and the truncated one (UDT*).

Thermal parameters	Decupled Approach[a] (reference)	UDT	UDT*	UDT Deviations (%)	UDT* Deviations (%)
U ($W\,m^{-2}\,K^{-1}$)	0.202 (±3.5%)	0.194	0.194	-4.16	-4.16
Y_{ie} ($W\,m^{-2}\,K^{-1}$)	0.195 (±14.0%)	0.188	0.188	-3.52	-3.52
f (-)	0.934 (±13.6%)	0.972	0.971	+4.04	+4.00
$\Delta\tau_{ie}$ (h)	1.33 (±1.2%)	1.43	1.43	+7.50	+7.50

[a] Results reported with the experimental measurement's uncertainty.

- Numerical and laboratory validations confirmed accuracy and consistency with reference values and conventional methods.
- The procedure bridges theoretical response-factor approaches with practical testing, offering a simplified yet comprehensive characterization of opaque components.

Although validated here on homogeneous walls, the method is not limited to such cases. It can be applied to multilayer or heterogeneous assemblies provided the measurement area is dominated by one-dimensional heat flux and free of significant thermal bridges. Similarly, air cavities do not represent an intrinsic limitation: stagnant air layers behave as an additional resistance, while ventilated cavities can be addressed by evaluating airflow and placing sensors accordingly. Future work will extend validation to more complex wall configurations and field-testing scenarios.

In conclusion, the UDT procedure represents a significant advancement in thermal characterization, offering a robust, efficient, and potentially standardizable approach to assessing building envelope performance. By enabling the extraction of both steady-state and periodic parameters from a single test, it has the potential to simplify practice, accelerate testing, and support more effective strategies for energy efficiency and sustainability in buildings.

CRediT authorship contribution statement

Maja Danovska: Writing – original draft, Visualization, Validation, Software, Methodology, Investigation, Formal analysis, Data curation, Conceptualization. **Davide Cassol:** Writing – review & editing, Visualization, Validation, Software, Methodology, Investigation, Formal analysis, Data curation, Conceptualization. **Ivan Giongo:** Writing – review & editing. **Alessandro Prada:** Writing – review & editing, Conceptualization.

Declaration of competing interest

The authors declare that they have no known competing financial interests or personal relationships that could have appeared to influence the work reported in this paper.

Data availability

Data will be made available on request.

References

[1] M. González-Torres, L. Pérez-Lombard, J. F. Coronel, I. R. Maestre, and D. Yan, "A review on buildings energy information: Trends, end-uses, fuels and drivers," Energy Reports, vol. 8. Elsevier Ltd, pp. 626–637, Nov. 01, 2022. doi: 10.1016/j.egyr.2021.11.280.
[2] D. Zhou, C. Y. Zhao, and Y. Tian, "Review on thermal energy storage with phase change materials (PCMs) in building applications," Applied Energy, vol. 92. Elsevier Ltd, pp. 593–605, 2012. doi: 10.1016/j.apenergy.2011.08.025.
[3] M. Saffari, C. Roe, D.P. Finn, Improving the building energy flexibility using PCM-enhanced envelopes, Appl. Therm. Eng. 217 (Nov. 2022), https://doi.org/10.1016/j.applthermaleng.2022.119092.
[4] P. Wang, Z. Liu, R. Liu, F. Zhang, L. Zhang, Energy flexibility of PCM-integrated building: Combination parameters design and operation control in multi-objective optimization considering different stakeholders, Energy 268 (Apr. 2023), https://doi.org/10.1016/j.energy.2023.126753.
[5] J. Kośny et al., "Dynamic Thermal Performance Analysis of PCM Products Used for Energy Efficiency and Internal Climate Control in Buildings," Buildings, vol. 13, no. 6, Jun. 2023, doi: 10.3390/buildings13061516.
[6] H. ur Rehman and A. Hasan, "Energy Flexibility and towards Resilience in New and Old Residential Houses in Cold Climates: A Techno-Economic Analysis," Energies (Basel), vol. 16, no. 14, Jul. 2023, doi: 10.3390/en16145506.
[7] Z. Du, G. Liu, X. Huang, T. Xiao, X. Yang, Y.L. He, Numerical studies on a fin-foam composite structure towards improving melting phase change, Int. J. Heat Mass Transf. 208 (Jul. 2023), https://doi.org/10.1016/j.ijheatmasstransfer.2023.124076.
[8] A. Arteconi, A. Mugnini, F. Polonara, Energy flexible buildings: a methodology for rating the flexibility performance of buildings with electric heating and cooling systems, Appl. Energy 251 (Oct. 2019), https://doi.org/10.1016/j.apenergy.2019.113387.

[9] V. Sambou, B. Lartigue, F. Monchoux, M. Adj, Thermal optimization of multilayered walls using genetic algorithms, Energy Build. 41 (10) (Oct. 2009) 1031–1036, https://doi.org/10.1016/j.enbuild.2009.05.007.
[10] L. Bellahcene, A. Cheknane, S.M.A. Bekkouche, D. Sahel, "The effect of the thermal inertia on the thermal transfer in building wall," in E3S Web of Conferences, EDP Sciences (Nov. 2017), https://doi.org/10.1051/e3sconf/20172200013.
[11] N. Aste, A. Angelotti, M. Buzzetti, The influence of the external walls thermal inertia on the energy performance of well insulated buildings, Energy Build. 41 (11) (Nov. 2009) 1181–1187, https://doi.org/10.1016/j.enbuild.2009.06.005.
[12] J. Le Dréau, P. Heiselberg, Energy flexibility of residential buildings using short term heat storage in the thermal mass, Energy 111 (Sep. 2016) 991–1002, https://doi.org/10.1016/j.energy.2016.05.076.
[13] G. Reynders, T. Nuytten, D. Saelens, Potential of structural thermal mass for demand-side management in dwellings, Build. Environ. 64 (Jun. 2013) 187–199, https://doi.org/10.1016/j.buildenv.2013.03.010.
[14] Z. Wei, J. Calautit, Predictive control of low-temperature heating system with passive thermal mass energy storage and photovoltaic system: Impact of occupancy patterns and climate change, Energy 269 (Apr. 2023), https://doi.org/10.1016/j.energy.2023.126791.
[15] S.Ø. Jensen, et al., IEA EBC Annex 67 Energy flexible buildings, Energy Build. 155 (Nov. 2017) 25–34, https://doi.org/10.1016/j.enbuild.2017.08.044.
[16] F. Lu, Z. Yu, Y. Zou, X. Yang, Cooling system energy flexibility of a nearly zero-energy office building using building thermal mass: potential evaluation and parametric analysis, Energy Build. 236 (Apr. 2021), https://doi.org/10.1016/j.enbuild.2021.110763.
[17] J. Lind, E. Möllerström, H. Averfalk, and F. Ottermo, "Energy flexibility using the thermal mass of residential buildings," Energy and Buildings, vol. 301. Elsevier Ltd, Dec. 15, 2023. doi: 10.1016/j.enbuild.2023.113698.
[18] H. Wolisz, A. Constantin, R. Streblow, and D. Mueller, "Performance assessment of heat distribution systems for sensible heat storage in building thermal mass," 2013. [Online]. Available: https://www.researchgate.net/publication/284413833.
[19] H. Li, Z. Wang, T. Hong, and M. A. Piette, "Energy flexibility of residential buildings: A systematic review of characterization and quantification methods and applications," Advances in Applied Energy, vol. 3. Elsevier Ltd, Aug. 25, 2021. doi: 10.1016/j.adapen.2021.100054.
[20] European Committee for Standardization, EN ISO 6946:2018 – Building components and building elements – Thermal resistance and thermal transmittance – Calculation methods (ISO 6946:2017), 2018.
[21] European Committee for Standardization, EN ISO 13786:2008 – Thermal performance of building components – Dynamic thermal characteristics – Calculation methods (ISO 13786:2007), 2008.
[22] E. Lucchi, Thermal transmittance of historical brick masonries: a comparison among standard data, analytical calculation procedures, and in situ heat flow meter measurements, Energy Build. 134 (Jan. 2017) 171–184, https://doi.org/10.1016/j.enbuild.2016.10.045.
[23] F. Asdrubali, G. Baldinelli, Thermal transmittance measurements with the hot box method: Calibration, experimental procedures, and uncertainty analyses of three different approaches, Energy Build. 43 (7) (Jul. 2011) 1618–1626, https://doi.org/10.1016/j.enbuild.2011.03.005.
[24] M. Danovska, G. Pernigotto, P. Baggio, A. Gasparella, Simulation uncertainty in heat transfer across timber building components in the italian climates: the role of thermal conductivity, Energy Build. 268 (Aug. 2022), https://doi.org/10.1016/j.enbuild.2022.112190.
[25] A. Prada, D. Gigli S., A. Gasparella, and M. Baratieri, "Energy simulation and design of a hot box suitable for dynamic tests of building envelope opaque components," 2013. [Online]. Available: www.unibz.it/universitypress.
[26] European Committee for Standardization, 1998. EN 1934:1998 – Thermal performance of buildings – Determination of thermal resistance by hot box method using heat flow meter – Masonry.
[27] B.S. Institution, Bs en sio,, — thermal insulation — Determination of steady-state thermal transmission properties — Calibrated and guarded hot box, British Standards Institution 8990 (1996) 1996.
[28] K. Trgala, M. Pavelek, R. Wimmer, Energy performance of five different building envelope structures using a modified Guarded Hot Box apparatus—Comparative analysis, Energy Build. 195 (Jul. 2019) 116–125, https://doi.org/10.1016/j.enbuild.2019.04.036.
[29] M. Calis, Change of U-value with extreme temperatures on different types of block walls, Journal of Building Engineering 85 (May 2024), https://doi.org/10.1016/j.jobe.2024.108653.
[30] W. Brown, "A guarded hot box procedure for determining the dynamic response of full-scale wall specimens-Part I." [Online]. Available: http://www.nrc-cnrc.gc.ca/irchttp://laws.justice.gc.ca/en/showtdm/cs/C-42http://lois.justice.gc.ca/fr/showtdm/cs/C-42.
[31] Brown, WC, Stephenson, and DG, "Guarded hot box measurements of the dynamic heat transmission characteristics of seven wall specimens - Part II." [Online]. Available: http://www.nrc-cnrc.gc.ca/irchttp://laws.justice.gc.ca/en/showtdm/cs/C-42http://lois.justice.gc.ca/fr/showtdm/cs/C-42.
[32] K. Ulgen, "Experimental and theoretical investigation of effects of wall's thermophysical properties on time lag and decrement factor.".
[33] G. Pernigotto, A. Prada, F. Patuzzi, M. Baratieri, A. Gasparella, "Characterization of the dynamic thermal properties of the opaque elements through experimental and numerical tests," in Energy Procedia, Elsevier Ltd (Nov. 2015) 3234–3239, https://doi.org/10.1016/j.egypro.2015.11.786.
[34] G. Pernigotto, A. Prada, M. Baratieri, and A. Gasparella, "Experimental characterization of the dynamic thermal properties of opaque elements under dynamic periodic solicitation," 2015, Accessed: Mar. 21, 2024. [Online]. Available: www.unibz.it/universitypress.
[35] N. Bishara, G. Pernigotto, A. Prada, M. Baratieri, A. Gasparella, Experimental determination of the building envelope's dynamic thermal characteristics in consideration of hygrothermal modelling – Assessment of methods and sources of uncertainty, Energy Build. 236 (Apr. 2021), https://doi.org/10.1016/j.enbuild.2021.110798.
[36] E. Gengembre, K. Jacquemet, "Static and dynamic thermal characterization of facade with mineral foam insulation using a hot-box apparatus," in Journal of Physics: Conference Series, Institute of Physics (Dec. 2021), https://doi.org/10.1088/1742-6596/2069/1/012089.
[37] G. P. Mitalas and D. G. Stephenson, "ROOM THERMAL RESPONSE FACTORS," 1967.
[38] K. Martín, I. Flores, C. Escudero, A. Apaolaza, J.M. Sala, Methodology for the calculation of response factors through experimental tests and validation with simulation, Energy Build. 42 (4) (Apr. 2010) 461–467, https://doi.org/10.1016/j.enbuild.2009.10.015.
[39] J.M. Sala, A. Urresti, K. Martín, I. Flores, A. Apaolaza, Static and dynamic thermal characterisation of a hollow brick wall: Tests and numerical analysis, Energy Build. 40 (8) (2008) 1513–1520, https://doi.org/10.1016/j.enbuild.2008.02.011.
[40] A. Rasooli, L. Itard, C.I. Ferreira, A response factor-based method for the rapid in-situ determination of wall's thermal resistance in existing buildings, Energy Build. 119 (May 2016) 51–61, https://doi.org/10.1016/j.enbuild.2016.03.009.
[41] A. Rasooli, L. Itard, In-situ rapid determination of walls' thermal conductivity, volumetric heat capacity, and thermal resistance, using response factors, Appl. Energy 253 (Nov. 2019), https://doi.org/10.1016/j.apenergy.2019.113539.
[42] C. Wang, X. Fu, X. Tao, X. Li, J. An, A Novel Response Factor-based Method for In Situ Measurement of Wall thermal Resistance, Buildings 13 (8) (2023) Aug, https://doi.org/10.3390/buildings13081986.
[43] G. Baldinelli, F. Bianchi, A.A. Lechowska, J.A. Schnotale, Dynamic thermal properties of building components: Hot box experimental assessment under different solicitations, Energy Build. 168 (Jun. 2018) 1–8, https://doi.org/10.1016/j.enbuild.2018.03.001.
[44] M.G. Davies, Building heat transfer, John Wiley & Sons, 2004.
[45] D. G. Stephenson and G. P. Mitalas, "Cooling Load Calculations by Thermal Response Factor Method.".
[46] D. HIttle, "RESPONSE FACTORS AND CONDUCTION TRANSFER FUNCTIONS." Accessed: Mar. 21, 2024. [Online]. Available: www.web.mit.edu.
[47] J.A. Clarke, Energy simulation in Building Design, Butterworth-Heinemann, 2001.
[48] MathWorks®, *fmisearch* algorithm " Search for local minimum of unconstrained multivariable function using derivative-free method" retrieved from: https://it.mathworks.com/help/matlab/ref/fminsearch.html?s_tid=srchtitle_site_search_1_fminsearch.
[49] COMSOL Multiphysics® software: https://www.comsol.com/.
[50] MATLAB®: https://it.mathworks.com/.